



# Treatment of burned soil leachates by ultrafiltration coupled with coagulation: Insights into membrane fouling

Sohail Farooq<sup>a</sup>, Ryan P. Cole<sup>b</sup>, Yuanchun Cao<sup>c</sup>, Madelyn L. Krebs<sup>d</sup>, Amanda K. Hohner<sup>e</sup>, Kevin D. Bladon<sup>b,f</sup>, Xue Jin<sup>a,\*</sup>

<sup>a</sup> School of Chemical, Biological, and Environmental Engineering, Oregon State University, Corvallis, OR 97331, USA

<sup>b</sup> Department of Forest Engineering, Resources, and Management, Oregon State University, Corvallis, OR, USA

<sup>c</sup> Department of Environmental Sciences, Oregon State University, Corvallis, OR, USA

<sup>d</sup> Department of Biochemistry and Biophysics, Oregon State University, Corvallis, OR, USA

<sup>e</sup> Department of Civil Engineering, Montana State University, Bozeman, MT, USA

<sup>f</sup> Department of Forest Ecosystems and Society, Oregon State University, Corvallis, OR, USA

## ARTICLE INFO

### Keywords:

Wildfire  
Climate change adaption  
Coagulation  
Membrane fouling

## ABSTRACT

This study evaluated the treatability of water leachates from wildfire-impacted soils using a coagulation-ultrafiltration process, aiming to better understand how post-fire changes affect membrane fouling in drinking water treatment. Soil samples were collected from one high burn severity and one low burn-severity site following the Cedar Creek Fire in Oregon, USA. The leachate from the one high severity site exhibited lower pH, turbidity, and dissolved organic carbon, and its dissolved organic matter (DOM) consisted of less aromatic compounds compared to the low-severity leachate. Filtration experiments revealed that, without pre-coagulation, the high-severity leachate caused less membrane fouling than the leachate from the low-severity sample. Pre-coagulation with aluminum chlorohydrate reduced fouling in both cases, though optimal dosages differed. For the low-severity leachate, a 30 mg/L dose improved DOM removal and minimized irreversible fouling, while for the high-severity leachate, effective control was observed at dosages up to 7.5 mg/L, with higher doses (30 mg/L) worsening fouling, potentially via metal-DOM complexes. While our controlled laboratory experiments provide valuable insights, we acknowledge that our lab experiments do not fully replicate field conditions. However, the unique characteristics of the leachate from our burned soil samples, indicate the need for further research to capture the complexities of post-wildfire water quality dynamics and refine treatment strategies for wildfire-impacted watersheds.

## 1. Introduction

Forested watersheds are the primary source of clean drinking water around the world (Costanza et al., 1997). In the United States, over 60 % of the potable water is supplied from forested areas (Smith et al., 2011; Stein, 2005). However, these water sources are increasingly at risk due to population growth and climate change, which expose them to both natural and human-made disturbances. One of the major concerns is wildfires, which rapidly consume biomass and transform forest vegetation into pyrogenic organic matter. This transformation can significantly alter the physical and chemical properties of the upper soil layers (Goforth et al., 2005; Oliveira-Filho et al., 2018; Santín et al., 2015;

Vergnoux et al., 2011; Wang et al., 2016). After a wildfire, hillslope runoff during storm events can transport large quantities of ash, charred biomass, and soil into the streams, rivers, and lakes within the burned watershed (Ryan et al., 2011; Minshall et al., 1997). Consequently, the water quality in the burned watershed can be altered, with elevated levels of particles (Murphy et al., 2012), heavy metals (Earl and Blinn, 2003), organics (Smith et al., 2011; Petticrew et al., 2006), and nutrients (Spencer et al., 2003). The extent of these changes in water quality often depends on the severity of the burn as well as the composition of the soil and ash (C. Santín et al., 2015). The postfire water quality changes can lead to significant challenges and concerns for downstream water treatment plants (Hohner et al., 2019).

\* Corresponding author at: School of Chemical, Biological, and Environmental Engineering, Oregon State University, 216 J Johnson Hall, Corvallis, OR 97331, USA.

E-mail address: [xue.jin@oregonstate.edu](mailto:xue.jin@oregonstate.edu) (X. Jin).

<https://doi.org/10.1016/j.wroa.2025.100357>

Received 9 April 2025; Received in revised form 14 May 2025; Accepted 23 May 2025

Available online 25 May 2025

2589-9147/© 2025 The Authors. Published by Elsevier Ltd. This is an open access article under the CC BY-NC license (<http://creativecommons.org/licenses/by-nc/4.0/>).

The application of low-pressure membranes (LPMs), including microfiltration and ultrafiltration, in drinking water treatment has grown rapidly over the past decade due to their effectiveness in producing high-quality water, compact footprint, and relatively low costs (Huang et al., 2009; Huang et al., 2022; Nakatsuka et al., 1996; Xu et al., 2019; Zularisam et al., 2009; Zhu et al., 2024). With pore sizes ranging from 10 to 100 nm, LPMs are highly efficient at removing particulates. However, they are ineffective at removing dissolved substances, and fouling remains a significant challenge that limits their performance. Fouling in LPMs is primarily caused by pore blocking and the formation of a cake layer (Wu et al., 2011; Wang and Tarabara, 2008; Xiong et al., 2025). To address these challenges, chemical coagulation pretreatment is specifically designed to improve membrane performance by (a) altering the size distribution of pollutants and (b) modifying the affinities of pollutants for one another and the membrane (Huang et al., 2009). The hybrid coagulation-LPM process aims to (1) enhance the removal of dissolved organic matter (DOM) and (2) mitigate membrane fouling (Kong et al., 2017). This treatment train is commonly employed in membrane-based drinking water treatment plants (Tran et al., 2022).

Wildfires can alter the chemical characteristics of particles and DOM, potentially reducing the effectiveness of the coagulation-LPM process. For example, the presence of smaller, more aromatic DOM in postfire water may lead to difficulties in coagulation, increased membrane fouling, and enhanced disinfection byproduct (DBP) formation (Emelko et al., 2011; Hohner et al., 2016; Chow et al., 1999). In regions affected by wildfires, the coagulation-LPM treatment process may face increased challenges to its resilience. However, there is a lack of comprehensive information on the effectiveness of this process for treating post-wildfire water, leading to substantial uncertainty about the potential challenges. As a first step towards filling the above knowledge gaps, we collected soil samples from a recently burned area and conducted laboratory experiments to explore the relationships between the composition of leachate from burned soil and the performance of the coagulation-LPM treatment process. We hypothesize that increased burn severity transforms soil DOM into smaller, less aromatic, and more hydrophilic fractions, which reduce coagulation efficacy and exacerbate irreversible membrane fouling through internal pore adsorption. The specific objectives of this research were to: (1) investigate the effects of burned soils leachate quality, specifically DOM characteristics, on the performance of the coagulation-ultrafiltration treatment process; (2) identify optimal coagulant dosages for effective DOM removal and membrane fouling control; and (3) characterize fouling mechanisms and dominant foulants through detailed membrane autopsy, including contact angle measurements and scanning electron microscopy-energy dispersive X-ray (SEM-EDS) analysis. This study is the first to investigate the impact of leachate from soils burned by wildfire on the performance of the coagulation-UF treatment process. The findings provide valuable insights to help utilities understand the potential challenges associated with operating efficient membrane-based drinking water treatment systems for treatment of post-wildfire water with degraded quality.

## 2. Materials and methods

### 2.1. Site description and sampling

The Cedar Creek wildfire, ignited by a lightning strike on August 1, 2022, burned a total of 45,441 hectares along the west slopes of the Cascade Mountains in Oregon before it was contained on November 22, 2022. The area includes diverse topographical and ecological features, with elevations ranging from 200 to 1600 m above sea level. The pre-fire vegetation primarily consisted of coniferous forests dominated by Douglas-fir (*Pseudotsuga menziesii*), western hemlock (*Tsuga heterophylla*), and western red cedar (*Thuja plicata*), interspersed with understory shrubs and grasses (USDA 2022). Soils in the region are predominantly Andisols, derived from volcanic ash deposits, and are characterized by high organic matter content and excellent water

retention capacity. The underlying geology includes basalt and andesite formations, with slopes ranging from gentle grades of 10 % to steeper inclines exceeding 60 % (Lake, 2003; Sytsma et al., 2005).

Soil and baseline water samples were collected in August 2023, within one year of the fire containment. Soil sampling focused on high- and low-severity burn areas, identified using burn severity maps and verified through field observations. Surface soils (top 3 cm) were collected with a clean trowel to target the layer most affected by fire and likely to erode during rainfall events. Sampling was conducted along 10-meter transects perpendicular to a stream channel, extending upslope from the stream edge. At each site, a measuring tape was laid out at a 90-degree angle to the stream, and soil samples were collected at specified intervals along this transect. Samples from high-severity burn areas were taken from dry stream beds and adjacent slopes, while low-severity burn samples were collected from areas with minimal fire impact (Figure S1, Supplementary Information). To prevent cross-contamination, gloves were worn during sampling, and tools were cleaned between collections.

To establish a baseline for leaching experiments, water samples were collected from Salmon Creek at a location approximately 1.5 m from the stream bank and just below the water surface, ensuring a steady flow. The carboy used for water collection was rinsed three times with creek water before being filled, sealed, and placed in a cooler for transport. Although no pre-fire data were available for Salmon Creek, post-fire measurements showed that its water exhibited low total organic carbon (TOC  $\approx 0.7$  mg/L), turbidity ( $\approx 0.3$  NTU) and conductivity ( $\approx 25$   $\mu$ S/cm). These characteristics made it suitable for use in leaching experiments where the goal was to assess how burned soil alter water chemistry. By starting with water that has minimal contamination, any increases in TOC, turbidity, or other parameters in the leachate could be attributed primarily to the influence of the burned soil, enabling a more accurate assessment of the soil's impact on water quality degradation (Blackburn et al., 2023; Fischer et al., 2023; Rodela et al., 2022; Swindle and al., 2021). Additionally, the presence of some electrolytes in the creek water, unlike deionized water, may better simulate natural leaching processes by facilitating the dissolution of organic matter from the soil. All soil and baseline water samples were stored in darkness at 4 °C to preserve their integrity prior to experiments.

### 2.2. Materials

All chemicals used in this study were either high-performance liquid chromatography grade or analytical grade. Aluminum chlorohydrate (ACH), which is the most common coagulant applied in membrane-based drinking water treatment plants, was purchased from Spectrum Chemical (Gardena, CA). The stock solution was prepared by dissolving 240 mg of ACH powder in 200 mL of deionized water. The ACH stock solution was freshly prepared before each experiment.

Flat sheet polyvinylidene difluoride (PVDF) membrane with a nominal molecular weight cut-off (MWCO) of 100 kDa was provided by Synder Filtration (Vacaville, CA). Prior to use, circular coupons with an effective surface area of 45 cm<sup>2</sup> were cut from a large sheet and soaked in deionized water for 24 h to wet the membrane and remove any preservative chemicals.

### 2.3. Experimental design

All experiments included replicated soil leachate preparation, treatments, and control tests, conducted under identical experimental conditions, except that no coagulant was added to the control tests. Data are reported as the mean  $\pm$  standard deviation from at least two independent replicate experiments. Figure S2 presents a schematic diagram of the leaching experiment, followed by the integrated coagulation-ultrafiltration (UF) treatment process.

#### 2.3.1. Experiment to prepare burned soil leachates

First, soils from the burned area were leached in the laboratory to

dissolve substances that could be released into nearby watersheds during or after precipitation at the wildfire site. This laboratory simulation aims to also represent the scenario in which these materials become entrained in the river and flow downstream to water treatment facilities (Hohner et al., 2016; Hohner et al., 2017). Leachates were prepared from soil samples collected at a high burn-severity site (location along 8 m transect) and a low burn-severity site (location along 8 m transect). To leach the soil samples, 5 g of soil per liter of baseline water were mixed for 24 h at 300 rpm at room temperature in the dark. A ratio of 5 g soil/L was selected to represent a scenario of severe water quality degradation after a wildfire event (Blackburn et al., 2023). Following the mixing, large particles were allowed to settle out of solution over a 30-minute period. The burned soil leachate was then subjected to the integrated coagulation–UF treatment.

### 2.3.2. Coagulation

The burned soil leachate was subjected to coagulation treatment using a six-paddle programmable jar test apparatus (Phipps and Bird Inc., Richmond, VA). ACH was selected as the coagulant, with dosages ranging from 0 to 30 mg/L. Following the addition of the coagulant, the suspensions were rapidly mixed at 300 rpm for 2 min, followed by a slow mixing phase at 50 rpm for 30 min. To simulate the inline coagulation process employed by most membrane-based water treatment facilities in Oregon, the resulting floc suspension was subsequently filtered through a steel mesh with a uniform sieve size of 254  $\mu\text{m}$  before moving into the UF feed water tank.

### 2.3.3. Ultrafiltration

Ultrafiltration experiments were conducted using a dead-end stirred cell system (Millipore, Billerica, MA). The effective filtration area of the cell was 45  $\text{cm}^2$ . Filtration was performed under constant pressure mode (40 psi) using a compressed nitrogen tank. A beaker was placed on a digital scale (OHAUS Navigator, NJ) to collect permeate samples. The change in weight was continuously recorded using a camera, and the membrane flux was determined from the weight changes over time. Fouling and cleaning experiments consisted of four steps: (1) compaction, (2) fouling, (3) backwashing, and (4) deionized water filtration. First, deionized water was filtered through the membranes at 40 psi until a stable flux was achieved. Second, the pre-coagulated postfire water was fed into the stirred cell, and filtration was conducted until 400 mL of permeate was collected. At the end of the fouling experiments, the stir cell was emptied and filled with deionized water. The fouled membrane was then flipped, and filtration was conducted until 400 mL of permeate was collected. After backwashing, the flux of deionized water was calculated again as a measure of flux recovery to determine fouling reversibility.

The distribution of membrane fouling resistance was analyzed by the resistance-in-series model shown below:

$$R_m = \frac{\Delta P}{\mu J_0} \quad (1)$$

$$R_{ir} = \frac{\Delta P}{\mu J_{DI}} - R_m \quad (2)$$

$$R_r = \frac{\Delta P}{\mu J_t} - R_m - R_{ir} \quad (3)$$

where  $\Delta P$  is the transmembrane pressure,  $\mu$  is the dynamic viscosity of the synthetic water;  $R_m$ ,  $R_{ir}$ ,  $R_r$  are the resistance of intrinsic membrane resistance, hydraulic irreversible resistance, and hydraulic reversible resistance, respectively;  $J_0$ ,  $J_{DI}$ ,  $J_t$  are the permeate flux of the pristine membrane, membrane after backwash, and membrane at the end of fouling test, respectively.

To identify the membrane fouling mechanism, a combined cake and standard blockage model was applied to describe the experimental data. This model accounts for the combined effects of (1) pore blockage,

which occurs when smaller particles block the membrane pores, and (2) cake layer formation, which begins when the pores are closed and particles start depositing on the membrane surface (Bolton et al., 2006). The model equations are described as follows:

$$V = \frac{2}{K_s} \left( \beta \cos \left( \frac{2\pi}{3} - \frac{1}{3} \arccos(\alpha) \right) + \frac{1}{3} \right) \quad (4)$$

$$\alpha = \frac{8}{27\beta^3} + \frac{4K_s}{3\beta^3 K_c J_0} + \frac{4k_s^2 t}{3\beta^3 K_c} \quad (5)$$

$$\beta = \sqrt{\frac{4}{9} + \frac{4K_s}{3K_c J_0} - \frac{2k_s^2 t}{3K_c}} \quad (6)$$

where,  $V$  is accumulative permeate volume,  $K_s$  is the standard blocking constant,  $K_c$  is the cake layer constant, and  $t$  is the filtration time. For curve fitting, we used the nonlinear least squares analysis method, implemented in MATLAB R2023b (MathWorks, Natick, MA). The accuracy of the model was evaluated based on the coefficient of determination ( $R^2$ ) value.  $R^2 \geq 0.98$  was considered as a successful fitting.

### 2.4. Water quality analysis

Samples were collected for water quality analysis from burned soil leachates, post-straining suspension, and UF permeate. Turbidity was measured using a portable turbidity meter (2100Q, Hach Company, CO). Particle size before and after coagulation was examined using a Laser Scattering Particle Size Distribution Analyzer (Partica LA-960, Horiba, Japan). Dissolved organic carbon (DOC) was analyzed using a Shimadzu TOC-L analyzer (Shimadzu Corp., Japan) after filtration through a 0.22  $\mu\text{m}$  polyethersulfone membrane. The filtration was carried out immediately after sampling. Concentrations of aluminum, iron, and silica in the leachates were quantified via inductively coupled plasma mass spectrometry (iCAP RQ ICP-MS, Thermo Fisher Scientific, MA).

In order to determine the composition of DOM, fluorescence excitation emission matrices (EEMs) and UV absorbance full scans were conducted using a fluorescence spectrophotometer (HORIBA Aqualog, Japan). The EEMs were obtained by measuring the fluorescence emission spectra wavelength (214–620 nm) and a range of excitation wavelength (240–600 nm) at 2 nm intervals. The scans were collected in signal/reference ratio mode with an integration time of 5 s. UV absorbance at 254 nm ( $\text{UV}_{254}$ ) was measured to assess the aromaticity of DOM. The specific UV absorbance ( $\text{SUVA}_{254}$ ) was calculated by dividing the  $\text{UV}_{254}$  absorbance by the DOC concentration (in mg/L). All the peaks of the DOM and slope ratio ( $\text{SR} = \text{Spectral slope}_{S_{275,295}} / \text{Spectral slope}_{S_{350,400}}$ ) were extracted and calculated from the contour graphs using fewsdm (Wampler, 2024) package in R software.

### 2.5. Membrane characterization

Pristine and fouled membranes were characterized using the following techniques. Surface hydrophobicity was evaluated via the sessile drop method using a contact angle goniometer (Ossila, England, UK). Zeta potentials were determined by streaming potential measurements, performed with the adjustable gap cell in the SurPASS system (Anton Paar, Austria). The zeta potential measurements were conducted in a 10 mM KCl solution with pH values ranging from 3 to 10. The membrane's top surface was visualized using an FEI Quanta 3D Field Emission Dual Beam Scanning Electron Microscope (SEM/FIB), equipped with a Horiba energy-dispersive X-ray (EDS) spectrometer (7200-H, Kyoto, Japan) for elemental composition analysis. Prior to SEM-EDS analysis, membrane samples were cut into small pieces, mounted on the specimen holder using double-sided tape, and sputter-coated with Au/Pd. Chemical functional groups on membrane surfaces were analyzed using Fourier-transform infrared spectroscopy (FTIR; Nicolet 6700, Thermo Fisher Scientific, MA) equipped with a 42° single-

reflection germanium attenuated total reflectance (ATR) element (Seagull™ variable angle reflection accessory).

### 3. Results and discussion

#### 3.1. Leachate water quality

In our study, leachate water quality was characterized to assess its impact on coagulation-UF treatment performance and membrane fouling potential. Leachates from low- and high-severity soils displayed distinct color variations (Fig. 1a). The leachate from the low-severity soil sample was dark black, whereas that from the high-severity soil sample was light reddish-brown. These color differences likely reflect variations in combustion completeness, as darker leachate from the low-severity burn soil suggests higher dissolved organic carbon content, while the lighter, reddish-brown leachate from the high-severity burn soil may indicate increased mineral leaching and oxidation. The iron-rich hue of high-severity burn leachate aligns with soil mineral transformations that occur over extended fire durations, rather than necessarily reflecting exposure to extreme heat. This is supported by XRD analysis, which identified the presence of iron oxides such as hematite and maghemite in the high-severity burn soil sample (Figure S3, Supplementary Information) (Ketterings and Bigham, 2000).

As expected, the leachate turbidity levels were significantly higher than the baseline sample (0.3 NTU) (Fig. 1b). The low-severity burn leachate exhibited higher turbidity compared to the high-severity burn leachate. In low-severity burn leachate, the higher turbidity may be attributed to the release of fine particulates and high molecular weight organic matter (Qiu et al., 2019), whereas in high-severity burn leachate, the lower turbidity might result from the loss of organic constituents and the aggregation of clay and mineral particles (Figure S1d, Supplementary Information) (Thuile Bistarelli et al., 2021).

Initially, the baseline water had a pH of approximately 7.7 (Fig. 1b). However, after leaching soils from the low- and high-severity burned areas, the pH decreased to 7.6 and 7.3, respectively. This observed pH reduction could potentially be attributed to several factors, such as the

leaching of organic acids and changes in soil chemistry post-fire. Burned soils often contain elevated levels of soluble organic acids, such as fulvic and humic acids, which are byproducts of organic matter combustion. When these soils are leached, the organic acids dissolve into the water, leading to a decrease in pH. This phenomenon has been documented in previous studies (Bárcenas-Moreno et al., 2016; Revchuk and Suffet, 2014). Notably, the high-severity leachate exhibited a lower SUVA<sub>254</sub> value (~3 L/mg·m), indicating reduced aromaticity compared to the low-severity leachate. This SUVA<sub>254</sub> value suggests the presence of a mixture of hydrophobic and hydrophilic DOM fractions. It is important to note that hydrophilic organic acids, such as aliphatic acids and low-aromatic acids, do not strongly absorb at 254 nm and therefore contribute minimally to SUVA<sub>254</sub>, despite significantly reducing pH (Aiken et al., 1992; Wang et al., 2019). Consequently, the observed pH decrease in the high-severity leachate is most likely attributed to these non-aromatic, hydrophilic acidic components rather than traditional humic or fulvic acids. However, pH changes after a fire are multifaceted, with both decreases and increases reported in the literature (Bárcenas-Moreno et al., 2016; Garrido-Ruiz et al., 2023). Variations in fire severity, soil characteristics, environmental conditions, and the time elapsed between the fire and sample collection can result in different outcomes, highlighting the complexity of post-fire biogeochemical processes.

After the leaching experiment, DOC concentrations increased from 0.7 mg/L in the baseline water to 2.7 mg/L for low-severity soil and to 2.4 mg/L for high-severity soil, respectively. SUVA<sub>254</sub> value is used to assess the aromaticity and hydrophobicity of DOM. The SUVA<sub>254</sub> value for the low-severity leachate was approximately 5.2 L/mg·m, indicating a higher concentration of aromatic compounds, which tend to be more hydrophobic and have higher molecular weights (Weishaar et al., 2003). In contrast, the high-severity sample has a SUVA<sub>254</sub> of 3 L/mg·m, suggesting a mixture of hydrophilic and hydrophobic organic compounds with molecular weights ranging from low to high (Edzwald et al., 1985). This shift toward lower molecular weight DOM in the high-severity burned soil leachate is further supported by the spectral slope ratio (S<sub>R</sub>) results, which are inversely correlated with DOM molecular weight

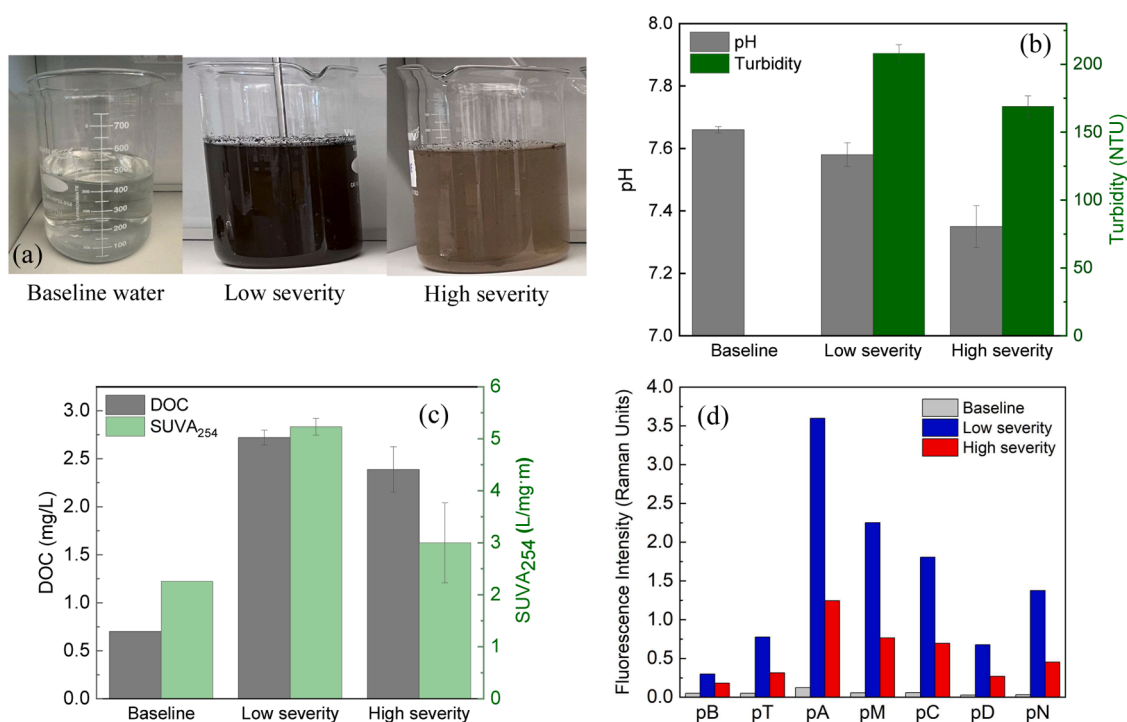


Fig. 1. Physical-chemical characteristics of baseline water and soil leachate: (a) photos, (b) turbidity and pH, (c) leachable dissolved organic carbon (DOC) and SUVA<sub>254</sub> and (d) fluorescence intensity. Error bars represent the standard deviation from two independent replicate experiments.

(Hansen et al., 2018). The higher  $S_R$  observed in the high-severity leachate ( $3.22 \pm 0.03$ ) compared to the low-severity leachate ( $2.85 \pm 0.02$ ) suggests a greater proportion of lower molecular weight DOM. These differences in DOM characteristics may be attributed to the degree of combustion severity. Low-severity burning often results in incomplete combustion, retaining larger, hydrophobic, humic-like organic compounds (Caon et al., 2014; Badía et al., 2014). In contrast, prolonged and more intense burning likely breaks down DOM into smaller, more soluble, and more hydrophilic fragments. This is consistent with the lower  $SUVA_{254}$  and higher  $S_R$  values observed in the high-severity leachate. Furthermore, the higher aromatic fraction in the low-severity leachate tends to remain in particulate/colloidal form for a longer duration, which also explains the higher turbidity observed in these samples (Fig. 1b) (Thuile Bistarelli et al., 2021).

EEMs collected with fluorescence spectroscopy uses fluorescence intensity of each wavelength pair to provide quantitative information about the corresponding DOM character and concentration. The raw EEMs contour plots are presented in Figure S4 (Supplementary Information). Peaks B (pB) and T (pT) represent protein-like substances, occurring at excitation/emission wavelengths of 270–280 nm / 300–320 nm and 270–280 nm / 320–350 nm, respectively. Peaks A (pA), M (pM), and C (pC) correspond to humic-like substances, detected at excitation/emission wavelengths of 250–260 nm / 380–480 nm, 310–320 nm / 380–420 nm, and 330–350 nm / 420–480 nm, respectively. Peak D (pD), observed at 390 nm / 509 nm, indicates soil fulvic acid-like substances. Peak N (pN), found at 280 nm / 370 nm, represents plankton-derived DOM (Coble, 2014). Both leachates were dominated by humic-like substances, indicating their ubiquitous presence in topsoil after fire (Revchuk and Suffet, 2014). The EEM results (Fig. 1d) also confirm the DOC results (Fig. 1c), showing that more DOM was leached into water from the low-severity burned soil compared to the high-severity sample.

In summary, the characterization of the burned soil leachates suggests that when an equivalent amount of soil is flushed into a nearby watershed, water leaching through soil from a high-severity burned area may exhibit lower pH, turbidity, and DOC than water leaching through soil from a low-severity burned area. Additionally, the composition of DOM may shift toward smaller, less aromatic organic compounds in high-severity areas compared to low-severity areas. However, it is important to note that in the field, high-severity burn areas can experience greater erosion, potentially leading to more soil being flushed into water bodies and resulting in higher DOC concentrations. In addition, we acknowledge that the findings presented here are based on a limited number of soil samples. Soils affected by wildfire are highly heterogeneous in both physical composition and burn severity. Therefore, while our results illustrate a clear pattern of how burn severity may influence leachate water quality, these findings should be interpreted as exploratory rather than conclusive. Further systematic studies with greater replication of soil samples across multiple locations within each burn severity category are necessary to validate these observations and to draw more robust conclusions about the effects of burn severity on leachate water quality and treatment implications.

### 3.2. Performance of coagulation

The performance of downstream UF treatment is highly dependent on effective coagulation. Failure to achieve optimal coagulation can result in poor solids removal and severe membrane fouling. Therefore, we begin with a discussion of the impact of leachate quality on coagulation efficiency. ACH is a widely used coagulant in water treatment because it (1) has high solubility and a strong positive charge, (2) performs well across a wide pH range, particularly in the neutral pH range where many water sources typically fall, and (3) produces less sludge compared to other coagulants, leading to more cost-effective sludge management (O'Melia, 1998). The dual mechanisms of charge neutralization and sweep flocculation allow ACH to effectively aggregate and remove a broad spectrum of impurities, including organic

matter, microorganisms, and turbidity (Zhang et al., 2017). The efficacy of coagulation with ACH for the removal of turbidity and DOM was evaluated in this section.

For the low and high burn severity soil leachates, coagulation followed by straining was not effective in removing suspended particles, with turbidity removal efficiency being less than 34 % (Fig. 2a). This is because the flocs formed by the ACH are compact (Figure S6) and most of the flocs cannot be removed by the 254  $\mu\text{m}$  screen (Tran et al., 2022). No sedimentation step was included to simulate inline coagulation, which would likely significantly reduce turbidity.

DOM can cause hydraulically irreversible membrane fouling (Kim and Dempsey, 2008). Coagulation plays a critical role in reducing DOM prior to UF, thereby mitigating fouling. In the low-severity leachate, increasing ACH doses progressively reduced DOC concentrations, achieving 36 % removal at 30 mg/L ACH (Figure 2b). As noted above, the high  $SUVA_{(254)}$  value (5.2 L/mg-m) indicates a dominance of aromatic, high-molecular-weight humic-like DOM, which responds well to ACH coagulation (Jeong et al., 2016), forming larger flocs that facilitate DOM removal by straining. The  $SUVA_{254}$  decreased by approximately 50 % at 30 mg/L ACH (Fig. 2c), confirming preferential removal of aromatic compounds known to contribute to fouling. EEMs analysis further corroborated these findings, showing substantial reductions in humic-like (peaks A, M, C) and fulvic-like (peak D) fluorescence intensities (Fig. 3a).

In contrast, the high-severity leachate exhibited a lower initial DOC (2.4 mg/L) and  $SUVA_{254}$  (3 L/mg-m), reflecting a shift toward smaller, more hydrophilic DOM. Although DOC removal increased with ACH dose, it was less pronounced than in the low-severity leachate, suggesting limited efficacy of ACH against hydrophilic, low-aromatic DOM. This behavior likely reflects the more aliphatic character of high-severity DOM, which is less responsive to charge neutralization and sweep flocculation. EEMs results confirmed weaker reductions in humic-like components, with fluorescence intensities stabilizing above 7.5 mg/L ACH (Figure 3b).

### 3.3. Effects of coagulant dose on UF membrane fouling

After coagulation and straining, the soil leachates were further treated by UF membrane. Membrane fouling was evaluated using normalized permeate flux profiles, the combined cake-standard blockage model, and the resistance-in-series model. Generally, flux declined immediately after introducing post-straining samples into the feed tank (Fig. 4). This initial rapid flux loss is likely attributed to pore blocking by small particles and DOM. As filtration progresses, a cake layer forms, further reducing flux as particles accumulate on the membrane surface (Abdelrasoul et al., 2013). Despite the baseline source water having turbidity of only 0.3 NTU and DOC of 0.7 mg/L, the baseline water showed a rapid initial flux loss followed by a minimal flux decline in the later stages of filtration. Photos of the fouled membrane surface show it appearing quite clean (Figure S8a). However, sub-micron colloidal particles (Figure S5, Supplementary Information) and DOM, which deposited within the membrane pores and are invisible to the naked eye, caused a 26.8 % flux decline by the end of filtration.

In contrast, the normalized permeate flux ( $J/J_0$ ) of the soil leachate without pre-coagulation decreased to 44.6 % (low severity) and 52.4 % (high severity) by the end of the filtration. Compared to baseline water, the increased turbidity and DOM of the soil leachates led to increased membrane fouling and flux decline. Interestingly, the flux decline was greater when treating the low-severity leachate compared to the high-severity leachate. This is not surprising because, without coagulation, the low-severity leachate had higher turbidity (Fig. 1b) and more DOM (Figs. 1c, 1d), which strongly correlates with membrane fouling (Xu et al., 2024). Consequently, the likelihood of both pore adsorption/clogging and cake layer formation is higher, resulting in more severe membrane fouling when treating the low severity leachate.

When ACH-treated samples were filtered, flux decline was lower

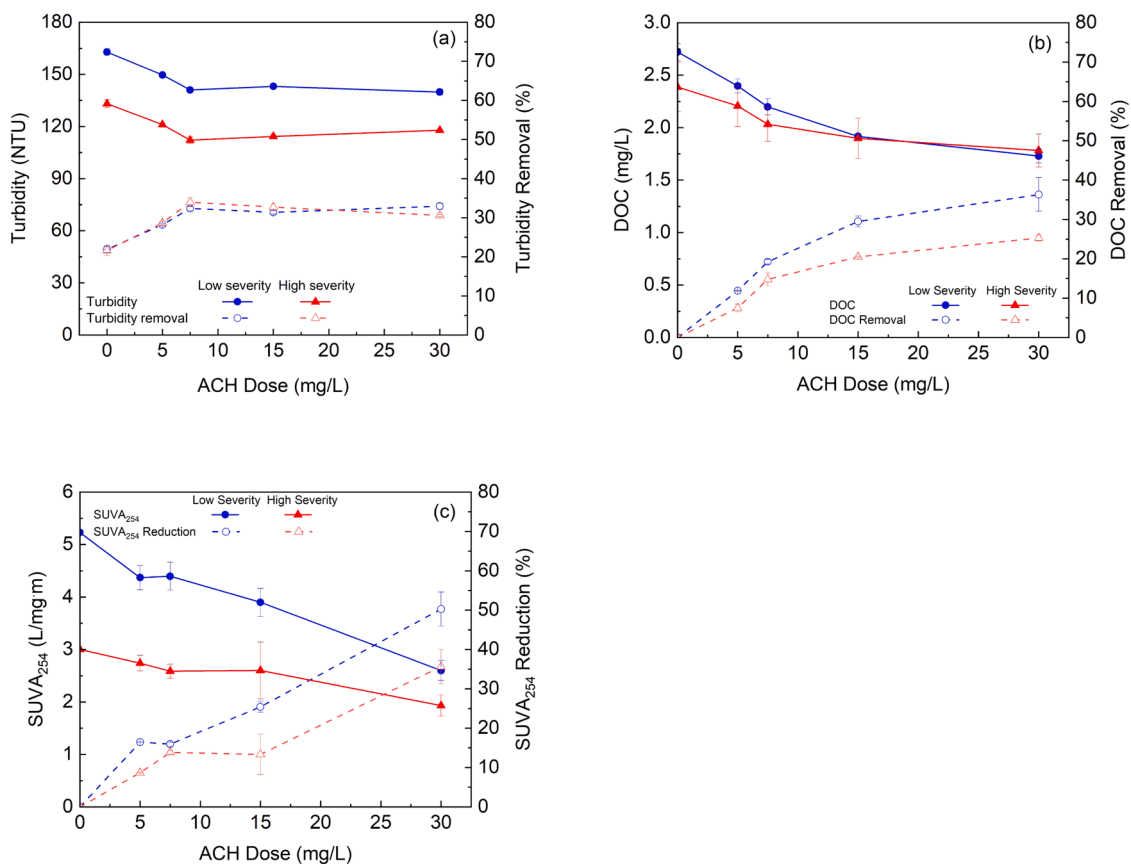


Fig. 2. (a) Turbidity removal (b) DOC removal and (c) SUVA<sub>254</sub> reduction after coagulation and straining.

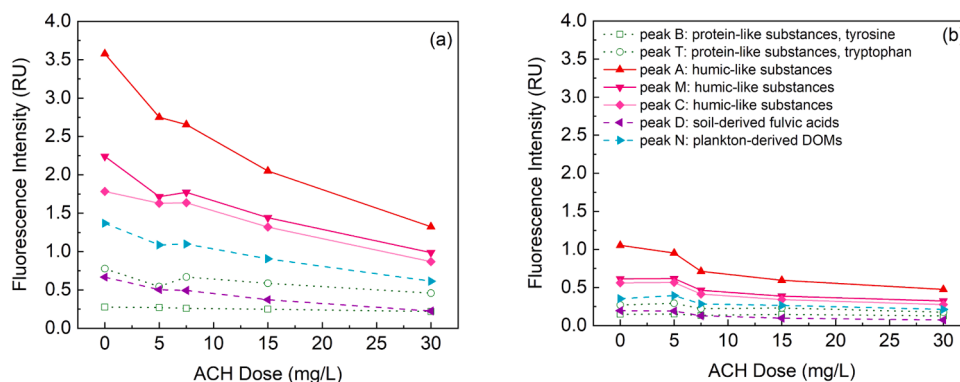


Fig. 3. Fluorescence intensity of major DOM components in soil leachate treated with ACH at varying dosages: (a) Low severity and (b) High severity.

than the corresponding values without pre-coagulation, verifying the effectiveness of ACH for fouling control in UF treatment (Tran et al., 2022). For the low-severity leachate, better fouling control performance was demonstrated at higher ACH doses. When 30 mg/L of ACH was applied, membrane fouling was reduced by 41.4%. For the high-severity leachate, the application of ACH at doses ranging from 5 to 15 mg/L reduced the flux decline. However, when the ACH dose was increased to 30 mg/L, the flux decline worsened to 53.7%, indicating an overdose of the coagulant. Optimal performance was achieved with a coagulant dose of 7.5 mg/L ACH, resulting in a 26.9% reduction in flux decline.

Our fouling experimental data fit well with the combined cake and standard blockage model (Table 1). According to the definitions of the fouling model, the individual contributions of standard blockage and cake layer formation to permeate flux decline can be evaluated from the magnitudes of the fitted parameters  $K_s$  and  $K_c$ , respectively. In almost all

conditions, ACH pre-coagulation led to reduced values of  $K_s$  and  $K_c$ , indicating alleviated pore clogging and cake layer formation.

After filtering the coagulated water, we performed a backwash to clean the membrane. Depending on its cleanability, membrane fouling can be classified as hydraulically reversible or irreversible. Reversible fouling is caused by the buildup of contaminant aggregates on the membrane surface, creating a cake layer with low hydraulic permeability. This type of fouling can be easily removed by physical cleaning methods, such as backwashing. In contrast, irreversible fouling occurs due to the adsorption of DOM and small particles within the membrane pores, necessitating chemical cleaning for removal (Kim and Dempsey, 2008). Irreversible fouling is a key performance-limiting challenge during long-term membrane filtration operations, as it requires harsh chemical cleaning, thereby increasing operating costs and leading to membrane degradation. In this study, the resistance-in-series model was

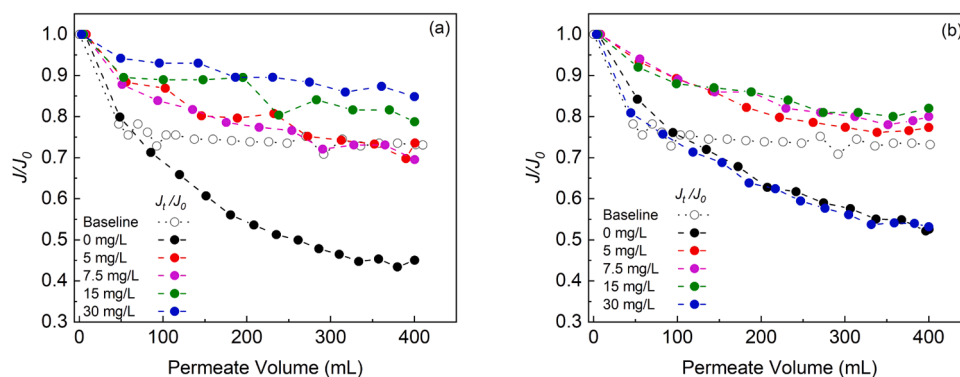


Fig. 4. Effect of ACH doses on flux decline during fouling experiments with (a) Low-severity leachate and (b) High-severity leachate.

Table 1

Fitting results of the combined cake-standard blockage model for uf process of postfire water with varying ACH Doses.

Low Burning Severity				
ACH dose [mg/L]	Model fit error, $R^2$	Characteristic parameters		
		$K_c$ ( $s/m^2$ )	$K_s$ (1/m)	$K_c J_0 / K_s$
0	0.9963	25,653	1.86	2.63
5	0.9926	18,601	1.74	2.12
7.5	0.9999	11,978	0.95	2.36
15	0.9999	7388	0.64	2.26
30	0.9999	5990	0.48	2.28
High Burning Severity				
ACH dose [mg/L]	Model fit error, $R^2$	Characteristic parameters		
		$K_c$ ( $s/m^2$ )	$K_s$ (1/m)	$K_c J_0 / K_s$
0	0.9934	19,163	1.27	2.6
5	0.9987	9199	0.73	2.3
7.5	0.9925	7832	0.64	2.29
15	0.9897	6692	0.54	2.36
30	0.9929	18,580	1.26	2.73

applied to further examine the impacts of burn severity and ACH pre-coagulation on reversible and irreversible fouling resistance created after the fouling experiment.

ACH pre-coagulation effectively controlled both reversible and irreversible fouling. For the low-severity leachate, increasing ACH dosage significantly reduced irreversible fouling resistance. With ACH doses reaching 30 mg/L, nearly all fouling became reversible. Membrane surface images (Figure S9e) revealed that most sediment was removed by backwashing. Contact angle measurements (Fig. 6) confirmed that the membrane regained its original hydrophobicity after

the fouling experiment with 30 mg/L ACH-coagulated low-severity leachate and subsequent backwashing. An ACH dose of 30 mg/L is considered optimal for the low-severity leachate coagulation, as it maximized DOM conversion to flocs (Fig. 2b and Fig. 3a). These large flocs effectively reduced internal pore clogging. Additionally, the minimal irreversible fouling suggests a weak adhesion force between the ACH flocs-induced cake layer and the membrane, facilitating its removal by backwashing.

For the high-severity leachate, ACH pre-coagulation reduced fouling, particularly reversible fouling, up to an ACH dose of 7.5 mg/L (Fig. 5b). Beyond this point, fouling reduction plateaued until 15 mg/L. However, further increasing the ACH dose to 30 mg/L resulted in a significant increase in both reversible and irreversible fouling. These findings highlight the importance of conducting a lab test to determine the optimal coagulant dosage when treating post-fire water, especially in cases of high-severity burning where changes in water composition can lead to coagulant overdosing, compared to water influenced by soils with low burn severity. After treating the high-severity leachate with 30 mg/L ACH pre-coagulation, the fouled membrane exhibited a positive surface charge within the pH range of 7–8 (Figure S11), indicating an overdose of positively charged aluminum species that deposited on the membrane surface.

Despite a lower optimal ACH dose for the high-severity leachate (7.5 mg/L) compared to the low-severity leachate (30 mg/L), irreversible fouling was more pronounced at the optimal dose for high-severity leachate. This observation suggests that high-severity burning alters soil and water chemistry, potentially increasing the proportion of hydrophilic organic substances. These hydrophilic compounds are less effectively removed by ACH coagulation and are more prone to interacting with and fouling the membrane surface. As shown in Fig. 6, the contact angle of the fouled membrane decreased to  $61.6^\circ$  when filtered with the relatively hydrophilic high-severity leachate (SUVA: 3 L/mg-m)

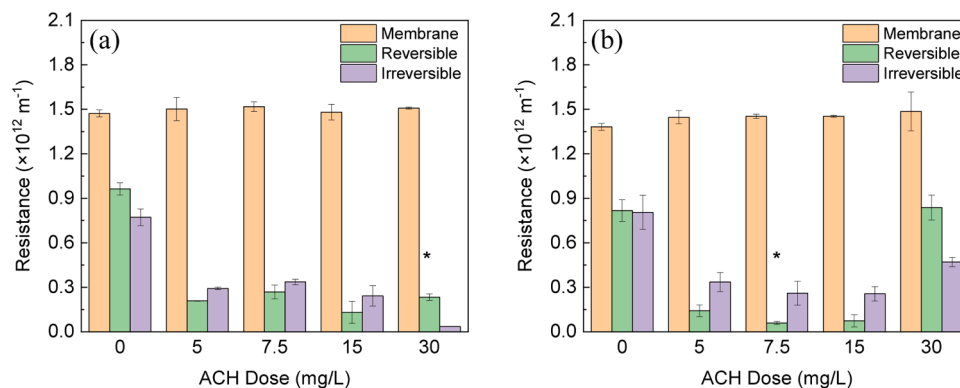


Fig. 5. Effect of ACH doses on membrane fouling reversibility for (a) Low and (b) High severity leachate (all experiments were conducted in duplicates). \* indicates optimal ACH dose.

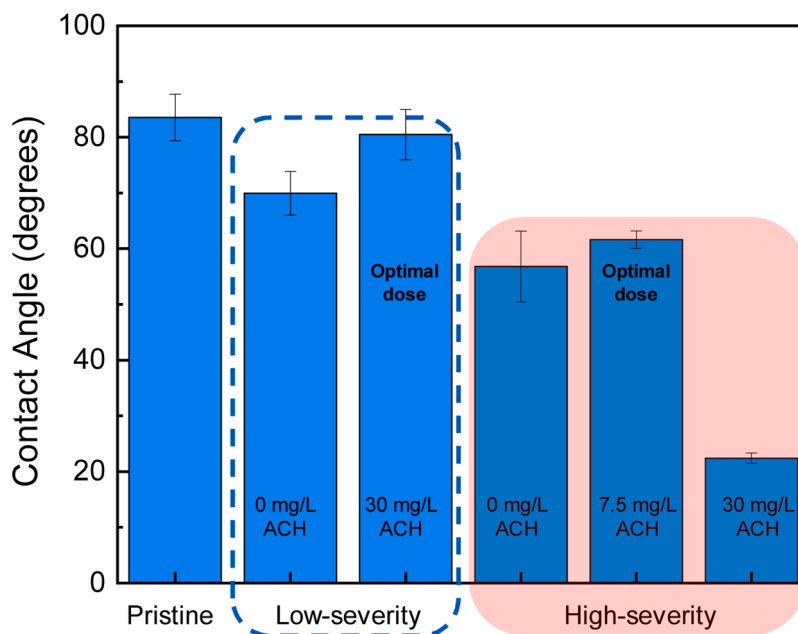


Fig. 6. Contact angle characterization of pristine and fouled membranes (After Backwashing).

at the optimal ACH dose. This reduction reflects the accumulation of hydrophilic substances on the membrane surface, contributing to irreversible fouling. While hydrophilic non-humic organics (e.g., amino sugars, as indicated by FTIR in Fig. 8) are likely contributors to the reduced contact angle, metal-associated DOM complexes (such as those with aluminum and iron) and silicate deposits identified in SEM-EDS analyses (Fig. 7) may also play a significant role in enhancing surface hydrophilicity (Lin et al., 2021; Khan et al., 2023). These substances, with lower molecular weight and fewer electron-rich sites compared to hydrophobic organic compounds, are less efficiently converted into flocs (A. Zularisam et al., 2007) and are more likely to deposit on the membrane surface (Lee et al., 2004). Furthermore, hydrophilic organic compounds and metals exhibit weaker electrostatic repulsion from the membrane, which facilitates their accumulation within membrane pores and the formation of a dense cake layer, ultimately leading to significant irreversible fouling (A. Zularisam et al., 2007). These findings align with

previous studies (A. Zularisam et al., 2007) which reported a higher fouling potential for source waters containing larger proportions of hydrophilic organics. The exact composition of DOM in the high-severity leachate requires further characterization using advanced techniques such as Fourier transform ion cyclotron resonance mass spectrometry (FT-ICR-MS), liquid chromatography–organic carbon detection (LC-OCD), and gel permeation chromatography (GPC).

The irreversible membrane fouling after treating the soil leachates and backwash was further investigated using SEM-EDS and FTIR to identify differences in surface morphology, elemental composition and functional groups. The pristine membrane was composed primarily of carbon and fluoride, consistent with the composition of PVDF membrane material (Fig. 7a). Its FTIR spectrum (Fig. 8) exhibited characteristic PVDF bands at  $3015\text{ cm}^{-1}$  and  $1400\text{ cm}^{-1}$  ( $-\text{CH}_2$  stretching) and at  $1275\text{ cm}^{-1}$  and  $1165\text{ cm}^{-1}$  ( $-\text{CF}_2$  vibrations), confirming a clean membrane surface. After treating the low-severity leachate with the optimal

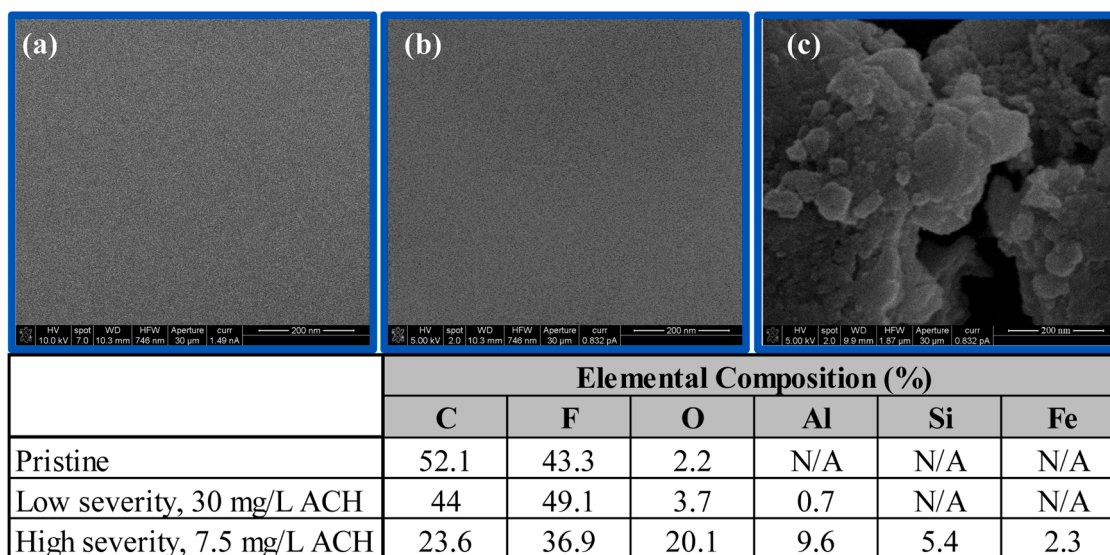


Fig. 7. SEM images and elemental analysis of the PVDF membrane top surface after backwashing: (a) pristine membrane; (b) membrane fouled by low-severity soil leachate following 30 mg/L ACH pre-coagulation; (c) membrane fouled by high-severity soil leachate following 7.5 mg/L ACH pre-coagulation.

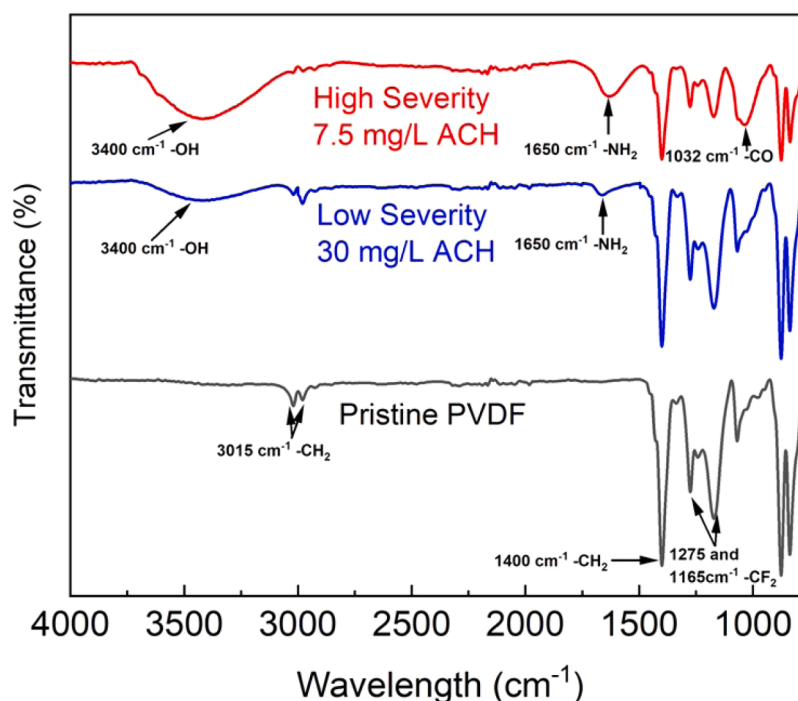


Fig. 8. FTIR Spectra of pristine and fouled membranes after backwash.

ACH dose (30 mg/L) and subsequent backwashing, the membrane surface exhibited minimal fouling, with only slight increases in oxygen and aluminum levels (Fig. 7b). Corresponding FTIR (Figure 8) detected modest new peaks at  $3400\text{ cm}^{-1}$  ( $-\text{OH}$ ) and  $1650\text{ cm}^{-1}$  ( $-\text{NH}_2$ ), indicating minor deposition of humic- and protein-like DOM (Zeng et al., 2016). In contrast, treatment of the high-severity leachate with the optimal ACH dose (7.5 mg/L) followed by backwashing resulted in a dense fouling layer covering most of the membrane surface (Fig. 7c). SEM-EDS revealed elevated levels of iron (Fe), aluminum (Al), silicon (Si), and oxygen (O). FTIR spectra of these fouled membranes exhibited strong peaks at  $3400\text{ cm}^{-1}$  ( $-\text{OH}$ ),  $1650\text{ cm}^{-1}$  ( $-\text{NH}_2$ ), and  $1032\text{ cm}^{-1}$  ( $-\text{C}-\text{O}$ ), indicating the accumulation of hydroxyl-, amine-, and carbonyl-rich DOM functional groups, which are likely involved in metal complexation (Zeng et al., 2016; Lee and Choi, 2022). The diminished intensity of native PVDF bands ( $1275$  and  $1165\text{ cm}^{-1}$  for  $-\text{CF}_2$ ) further confirmed extensive surface coverage by the fouling layer.

The presence of Fe and Al on the fouled membrane surface, along with the morphological and functional group changes observed in SEM images and FTIR analysis, indicates that these metals likely contributed to membrane fouling. Polyvalent metal ions, such as  $\text{Fe}^{3+}$  and  $\text{Al}^{3+}$ , are known to form complexes with hydrophilic DOM (e.g., polysaccharides), enhancing their adhesion to membrane surfaces. For instance, previous studies have demonstrated that iron can chelate with oxygen-containing functional groups, such as hydroxyl and carboxyl groups, in DOM to form stable complexes that are difficult to remove (Hao et al., 2013). These Fe/Al-DOM complexes can strongly adhere to the membrane, clog its pores, or form dense cake layers, ultimately leading to irreversible fouling. Additionally, the detection of Si and O on the fouled membrane surface suggests the potential contribution of silica ( $\text{SiO}_2$ ) or silicate compounds, likely originating from soil minerals, to the fouling process. Silica and silicate particles are known to exacerbate fouling by forming impermeable deposits.

Notably, SEM-EDS analysis revealed minimal metal-DOM complexes on membranes exposed to the low-severity leachate (Fig. 7b), despite its higher metal content (Table S1, Supplemental Information). This apparent paradox can be explained by the leachate's elevated  $\text{SUVA}_{254}$  ( $>5\text{ L}/\text{mg}\cdot\text{m}$ ), which is indicative of hydrophobic, aromatic DOM with limited solubility and metal-binding capacity. The reduced aqueous

interaction of hydrophobic DOM restricts its complexation with metal ions, resulting in minimal irreversible deposition on the membrane (Zhang et al., 2024). Conversely, the high-severity leachate ( $\text{SUVA}_{254} \sim 3\text{ L}/\text{mg}\cdot\text{m}$ ) contained hydrophilic, low-molecular-weight DOM enriched with carboxyl, phenolic, and hydroxyl groups (Fig. 8). These polar functional groups facilitated robust coordination with metal ions despite lower bulk metal concentrations, as evidenced by SEM-EDS-detected deposits (Fig. 7c). Thermal processes during high-severity burning may have enhanced metal reactivity, further promoting complexation with hydrophilic DOM (Zhang et al., 2024; Fernández et al., 1997). Together, these results demonstrate that irreversible fouling depends not only on metal concentration but also on DOM composition, metal speciation, and mineral content. The interplay between metal ions, DOM, and mineral-derived compounds highlights the complexity of fouling mechanisms in systems treating wildfire-impacted waters. To confirm the detailed bonding interactions of metal-DOM and metal-silicate complexes, future investigations should employ targeted spectroscopic techniques such as X-ray photoelectron spectroscopy (XPS) and X-ray absorption near edge structure (XANES) (Hay and Myneni, 2010; Chen et al., 2020; Daugherty et al., 2017).

#### 4. Conclusion

To the best of our knowledge, this is the first study to investigate the membrane fouling behavior and reversibility during the treatment of burned soil leachates. The primary findings are as follows:

1. Soil leachate from a high-severity burn site exhibited lower pH, turbidity, and DOC concentrations compared to the soil leachate from a low-severity burn site, with DOM shifting toward smaller, less aromatic compounds.
2. The low-severity leachate demonstrated a higher fouling potential due to the greater turbidity and DOM content in the absence of pre-coagulation.
3. A combined cake and standard blockage model revealed that both pore clogging and cake layer formation contribute to membrane fouling.

- For the low-severity leachate, increasing ACH dosage improved the removal of dissolved humic-like substances before ultrafiltration, reducing fouling, especially irreversible fouling.
- For the high-severity leachate, ACH was less effective in controlling irreversible fouling due to its insufficient removal of problematic foulant (e.g., hydrophilic DOM, metal-DOM complexes, SiO<sub>2</sub>). This finding suggests that alternative coagulants (e.g., biopolymer chitosan) should be considered for treating water draining from watersheds impacted by high-severity wildfires.

While these findings provide critical insights into the influence of fire severity on leachate composition and membrane fouling; however, limitations include a restricted sample set and laboratory-scale conditions that may not capture field variability. Future research should incorporate diverse soils across burn severities and geographies, assess long-term biofouling dynamics, and evaluate the roles of soil properties, geologic context, and postfire interval to inform robust, field-relevant water treatment strategies.

### CRedit authorship contribution statement

**Sohail Farooq:** Writing – original draft, Investigation, Formal analysis. **Ryan P. Cole:** Methodology. **Yuanchun Cao:** Investigation. **Madelyn L. Krebs:** Investigation. **Amanda K. Hohner:** Writing – review & editing, Methodology, Funding acquisition, Formal analysis. **Kevin D. Bladon:** Writing – review & editing, Supervision, Resources, Methodology, Funding acquisition, Formal analysis, Conceptualization. **Xue Jin:** Writing – review & editing, Supervision, Funding acquisition, Formal analysis.

### Declaration of competing interest

The authors declare that they have no known competing financial interests or personal relationships that could have appeared to influence the work reported in this paper.

### Acknowledgements

This work was supported by the U.S. Forest Service agreement 22-JV-11261952-071 and 23-JV-11261954-057. The authors are grateful to Drs. Kyle K. Shimabuku, Steve Wondzell, Sonja H. Kolstoe for their guidance and discussions. The authors would thank Dr. Salini Sasidharan for providing access to the Partica LA-960 Particle Size Analyzer.

### Supplementary materials

Supplementary material associated with this article can be found, in the online version, at [doi:10.1016/j.wroa.2025.100357](https://doi.org/10.1016/j.wroa.2025.100357).

### Data availability

Data will be made available on request

### References

- Abdelrasoul, A., Doan, H., Lohi, A., 2013. Fouling in membrane filtration and remediation methods. *Mass Transf. Adv. Sustain. Energy Environ. Oriented Numer. Model.*
- Aiken, G.R., et al., 1992. Isolation of hydrophilic organic acids from water using nonionic macroporous resins. *Org. Geochem.* 18 (4), 567–573.
- Badía, D., et al., 2014. Wildfire effects on nutrients and organic carbon of a rendzic phaeozem in NE Spain: changes at cm-scale topsoil. *Catena* 113, 267–275.
- Bárceñas-Moreno, G., et al., 2016. Plant community influence on soil microbial response after a wildfire in Sierra Nevada National Park (Spain). *Sci. Total. Environ.* 573, 1265–1274.
- Blackburn, E.A., et al., 2023. Biological filtration is resilient to wildfire ash-associated organic carbon threats to drinking water treatment. *ACS Est. Water* 3 (3), 639–649.
- Bolton, G., LaCasse, D., Kuriyel, R., 2006. Combined models of membrane fouling: development and application to microfiltration and ultrafiltration of biological fluids. *J. Memb. Sci.* 277 (1–2), 75–84.
- Caon, L., et al., 2014. Effects of wildfire on soil nutrients in Mediterranean ecosystems. *Earth-Sci. Rev.* 139, 47–58.
- Chen, H., et al., 2020. XPS and two-dimensional FTIR correlation analysis on the binding characteristics of humic acid onto kaolinite surface. *Sci. Total. Environ.* 724, 138154.
- Chow, C., et al., 1999. The impact of the character of natural organic matter in conventional treatment with alum. *Water. Sci. Technol.* 40 (9), 97–104.
- Coble, P.G., 2014. *Aquatic Organic Matter Fluorescence*. Cambridge University Press.
- Costanza, R., et al., 1997. The value of the world's ecosystem services and natural capital. *Nature* 387 (6630), 253–260.
- Daugherty, E.E., et al., 2017. Complexation and redox buffering of iron (II) by dissolved organic matter. *Env. Sci. Technol.* 51 (19), 11096–11104.
- Earl, S.R., Blinn, D.W., 2003. Effects of wildfire ash on water chemistry and biota in South-Western USA streams. *Freshw. Biol.* 48 (6), 1015–1030.
- Edzwald, J.K., Becker, W.C., Wattier, K.L., 1985. Surrogate parameters for monitoring organic matter and THM precursors. *J. Am. Water Works Assoc.* 77 (4), 122–132.
- Emelko, M.B., et al., 2011. Implications of land disturbance on drinking water treatability in a changing climate: demonstrating the need for “source water supply and protection” strategies. *Water. Res.* 45 (2), 461–472.
- Fernández, I., Cabaneiro, A., Carballas, T., 1997. Organic matter changes immediately after a wildfire in an Atlantic forest soil and comparison with laboratory soil heating. *Soil. Biol. Biochem.* 29 (1), 1–11.
- Fischer, S.J., et al., 2023. Fluorescence and absorbance indices for dissolved organic matter from wildfire ash and burned watersheds. *ACS. ES. T. Water.* 3 (8), 2199–2209.
- Garrido-Ruiz, C., et al., 2023. Effect of wildfires on soil properties of agricultural lands of Mediterranean-climate region in Chile. *Chil. J. Agric. Res.* 83 (6), 643–655.
- Goforth, B.R., et al., 2005. Spatial distribution and properties of ash and thermally altered soils after high-severity forest fire, southern California. *Int. J. Wildland. Fire* 14 (4), 343–354.
- Hansen, A.M., et al., 2018. Procedures for using the Horiba Scientific Aqualog® fluorometer to measure absorbance and fluorescence from dissolved organic matter. US Geological Survey.
- Hao, Y., et al., 2013. Effect of metal ions on the protein fouling of hollow-fiber ultrafiltration membranes. *Sep. Purif. Technol.* 111, 137–144.
- Hay, M.B., Myneni, S.C., 2010. X-ray absorption spectroscopy of aqueous aluminum-organic complexes. *J. Phys. Chem. A* 114 (20), 6138–6148.
- Hohner, A.K., et al., 2016. Drinking water treatment response following a Colorado wildfire. *Water. Res.* 105, 187–198.
- Hohner, A.K., et al., 2017. Water treatment process evaluation of wildfire-affected sediment leachates. *Environ. Sci.: Water Res. Technol.* 3 (2), 352–365.
- Hohner, A.K., et al., 2019. Wildfires alter forest watersheds and threaten drinking water quality. *Acc. Chem. Res.* 52 (5), 1234–1244.
- Huang, H., Schwab, K., Jacangelo, J.G., 2009. Pretreatment for low pressure membranes in water treatment: a review. *Env. Sci. Technol.* 43 (9), 3011–3019.
- Huang, Z., et al., 2022. Fabrication of fibrous MXene nanoribbons (MNRs) membrane with efficient performance for oil-water separation. *J. Memb. Sci.* 661, 120949.
- Jeong, S., et al., 2016. Removal of natural organic matter at the Gunbower water treatment plant in northern Victoria. *Aust. Desalin. Water Treat.* 57 (20), 9061–9069.
- Ketterings, Q.M., Bigham, J.M., 2000. Soil color as an indicator of slash-and-burn fire severity and soil fertility in Sumatra. *Indones. Soil Sci. Soc. Am. J.* 64 (5), 1826–1833.
- Khan, A., et al., 2023. Novel approach to landfill wastewater treatment fouling mitigation: air gap membrane distillation with tin sulfide-coated PTFE membrane. *Membrane* 13 (5), 483.
- Kim, H.C., Dempsey, B.A., 2008. Effects of wastewater effluent organic materials on fouling in ultrafiltration. *Water. Res.* 42 (13), 3379–3384.
- Kong, F.x., et al., 2017. Application of coagulation-UF hybrid process for shale gas fracturing flowback water recycling: performance and fouling analysis. *J. Memb. Sci.* 524, 460–469.
- Lake, Waldo, 2003. Report 15 - Civil & Environmental Engineering. Waldo Lake Research. Available from: <http://www.ce.pdx.edu/w2/download/waldo/Waldo%20Lake%20Report15.pdf>.
- Lee, H.K., Choi, S.J., 2022. Copper ferrocyanide chemically immobilized onto a polyvinylidene fluoride hollow-fibre membrane surface for the removal of aqueous cesium. *Env. Technol.* 43 (15), 2241–2251.
- Lee, N., et al., 2004. Identification and understanding of fouling in low-pressure membrane (MF/UF) filtration by natural organic matter (NOM). *Water. Res.* 38 (20), 4511–4523.
- Lin, Y.L., et al., 2021. Mitigating silica fouling and improving PPCP removal by modified NF90 using in situ radical graft polymerization. *Membrane* 11 (11), 904.
- Minshall, G.W., Robinson, C.T., Lawrence, D.E., 1997. Postfire responses of lotic ecosystems in Yellowstone National Park, USA. *Can. J. Fish. Aquat. Sci.* 54 (11), 2509–2525.
- Murphy, S.F., McCleskey, R.B., Writer, J.H., 2012. Effects of Flow Regime On Stream Turbidity and Suspended Solids After wildfire, Colorado Front Range. IAHS-AISH Publ.
- Nakatsuka, S., Nakate, I., Miyano, T., 1996. Drinking water treatment by using ultrafiltration hollow fiber membranes. *Desalination.* 106 (1–3), 55–61.
- Oliveira-Filho, E.C., et al., 2018. Effects of ashes from a Brazilian savanna wildfire on water, soil and biota: an ecotoxicological approach. *Sci. Total. Environ.* 618, 101–111.

- O'Melia, C.R., 1998. Coagulation and sedimentation in lakes, reservoirs and water treatment plants. *Water. Sci. Technol.* 37 (2), 129–135.
- Petticrew, E.L., Owens, P.N., Giles, T.R., 2006. Wildfire effects on the quantity and composition of suspended and gravel-stored sediments. *Interact. Between Sediments Water* 283–292.
- Qiu, F., et al., 2019. Impact of an extreme winter storm event on the coagulation/flocculation processes in a prototype surface water treatment plant: causes and mitigating measures. *Int J. Env. Res Public Health* 16 (15), 2808.
- Revchuk, A.D., Suffet, I., 2014. Effect of wildfires on physicochemical changes of watershed dissolved organic matter. *Water. Environ. Res.* 86 (4), 372–381.
- Rodela, M.H., Chowdhury, I., Hohner, A.K., 2022. Emerging investigator series: physicochemical properties of wildfire ash and implications for particle stability in surface waters. *Process. Impacts* 24 (11), 2129–2139.
- Ryan, S.E., Dwire, K.A., Dixon, M.K., 2011. Impacts of wildfire on runoff and sediment loads at Little Granite Creek, western Wyoming. *Geomorphology* 129 (1–2), 113–130.
- Santfín, C., et al., 2015a. Pyrogenic organic matter production from wildfires: a missing sink in the global carbon cycle. *Glob. Chang. Biol.* 21 (4), 1621–1633.
- Santfín, C., et al., 2015b. Quantity, composition and water contamination potential of ash produced under different wildfire severities. *Env. Res.* 142, 297–308.
- Smith, H.G., et al., 2011. Wildfire effects on water quality in forest catchments: a review with implications for water supply. *J. Hydrol.* 396 (1–2), 170–192.
- Spencer, C.N., Gabel, K.O., Hauer, F.R., 2003. Wildfire effects on stream food webs and nutrient dynamics in Glacier National Park. *USA. For. Ecol. Manag.* 178 (1–2), 141–153.
- Stein, S.M., 2005. *Forests On the edge: Housing Development On America's private Forests*, 636. US Department of Agriculture, Forest Service, Pacific Northwest Research Station.
- Swindle, C., et al., 2021. Effects of wildfires and ash leaching on stream chemistry in the Santa Ynez Mountains of Southern California. *Water.* 13 (17), 2402.
- Sytsma, M.D., et al., 2005. *Waldo Lake Research in 2004*.
- Thuile Bistarelli, L., et al., 2021. Wildfire-derived pyrogenic carbon modulates riverine organic matter and biofilm enzyme activities in an in situ flume experiment. *ACS Est. Water.* 1 (7), 1648–1656.
- Tran, Q.N., Jin, X., Doan, N.Q., 2022. Enhanced removal of extracellular microcystin-LR using chitosan coagulation-ultrafiltration: performance and mechanisms. *J. Environ. Chem. Eng.* 10 (3), 107902.
- USDA, 2022. *Burned-Area Report*. October 17 Available from: [https://www.fs.usda.gov/Internet/FSE\\_DOCUMENTS/fseprd1019126.pdf](https://www.fs.usda.gov/Internet/FSE_DOCUMENTS/fseprd1019126.pdf).
- Vergnoux, A., et al., 2011. Effects of forest fires on water extractable organic matter and humic substances from Mediterranean soils: uV-vis and fluorescence spectroscopy approaches. *Geoderma* 160 (3–4), 434–443.
- Wampler, K.A., 2024. *fewsdm: tools to process data from horiba aqualog*. R Package Version 1.1.2.
- Wang, F., Tarabara, V.V., 2008. Pore blocking mechanisms during early stages of membrane fouling by colloids. *J. Colloid. Interface Sci.* 328 (2), 464–469.
- Wang, J.J., et al., 2016. Temporal variations of disinfection byproduct precursors in wildfire detritus. *Water. Res.* 99, 66–73.
- Wang, W., et al., 2019. Isolation and characterization of hydrophilic dissolved organic matter in waters by ion exchange solid phase extraction followed by high resolution mass spectrometry. *Env. Chem Lett.* 17, 1857–1866.
- Weishaar, J.L., et al., 2003. Evaluation of specific ultraviolet absorbance as an indicator of the chemical composition and reactivity of dissolved organic carbon. *Env. Sci. Technol.* 37 (20), 4702–4708.
- Wu, J., et al., 2011. Modeling of the submerged membrane bioreactor fouling by the combined pore constriction, pore blockage and cake formation mechanisms. *Desalination.* 279 (1–3), 127–134.
- Xiong, L., et al., 2025. Bio-derived carboxymethyl cellulose-graft-gallic acid antiscalant with remarkable antibacterial activity for reverse osmosis scaling and biofouling control. *Water. Res.*, 123716
- Xu, D., et al., 2019. A comparison study of sand filtration and ultrafiltration in drinking water treatment: removal of organic foulants and disinfection by-product formation. *Sci. Total. Environ.* 691, 322–331.
- Xu, M., et al., 2024. New insights into membrane fouling in coagulation-ultrafiltration by cake characteristics analysis: a case study with PACl-A113 and PACl. *J. Environ. Sci.* 146, 217–225.
- Zeng, Z., et al., 2016. Graphene oxide quantum dots covalently functionalized PVDF membrane with significantly-enhanced bactericidal and antibiofouling performances. *Sci. Rep.* 6 (1), 20142.
- Zhang, D., et al., 2017. Influence of coagulation process on the ultrafiltration performance—the roles of Al species and characteristics of algae-laden water. *Sep. Purif. Technol.* 183, 32–42.
- Zhang, X., et al., 2024. Effects of Ca<sup>2+</sup> and Mg<sup>2+</sup> on Cu binding in hydrophilic and hydrophobic dissolved organic matter fractions extracted from agricultural soil. *Chemosphere* 352, 141441.
- Zhu, H., et al., 2024. Illuminating for purity: photocatalytic and photothermal membranes for sustainable oil-water separation. *Water. Res.*, 122919
- Zularisam, A., et al., 2007a. Fabrication, fouling and foulant analyses of asymmetric polysulfone (PSF) ultrafiltration membrane fouled with natural organic matter (NOM) source waters. *J. Memb. Sci.* 299 (1–2), 97–113.
- Zularisam, A., et al., 2007b. The effects of natural organic matter (NOM) fractions on fouling characteristics and flux recovery of ultrafiltration membranes. *Desalination.* 212 (1–3), 191–208.
- Zularisam, A., et al., 2009. Application of coagulation-ultrafiltration hybrid process for drinking water treatment: optimization of operating conditions using experimental design. *Sep. Purif. Technol.* 65 (2), 193–210.